

RESEARCH ARTICLE

10.1002/2017JD026528

Key Points:

- Early/fast VLF perturbations may be caused by sustained heating of the ionosphere by thunderstorm electrostatic fields
- These events are likely only detectable for low magnetic field dip angles or at low latitudes
- These events are more prominent for tenuous nighttime ionosphere profiles

Correspondence to:

R. A. Marshall,
robert.marshall@colorado.edu

Citation:

Kabirzadeh, R., R. A. Marshall, and U. S. Inan (2017), Early/fast VLF events produced by the quiescent heating of the lower ionosphere by thunderstorms, *J. Geophys. Res. Atmos.*, 122, doi:10.1002/2017JD026528.

Received 26 JAN 2017

Accepted 8 JUN 2017

Accepted article online 12 JUN 2017

Early/fast VLF events produced by the quiescent heating of the lower ionosphere by thunderstorms

R. Kabirzadeh¹, R. A. Marshall² , and U. S. Inan^{1,3}
¹Department of Electrical Engineering, Stanford University, Stanford, California, USA, ²Department of Aerospace Engineering Sciences, University of Colorado Boulder, Boulder, Colorado, USA, ³Department of Electrical Engineering, Koç University, Istanbul, Turkey

Abstract Large and easily distinguishable perturbations of the VLF transmitter signals due to interactions with thundercloud-driven ionospheric modifications have been observed and studied for about three decades. These events are called “early/fast VLF” or “early VLF” events due to their immediate detection (~20 ms) after the causative lightning flash on the ground and the fast rise time of the perturbed signal. Despite many years of study, the physical mechanisms responsible for these perturbations are still under investigation. Modifications of the sustained heating level of the ionosphere due to a lightning flash has been previously proposed as the causative mechanism of early/fast VLF events. The perturbations predicted by this mechanism, however, have been much smaller than experimental observations of 0.2–1 dB or higher. In this study, by using an improved 3-D thundercloud electrostatic upward coupling model which uses a realistic geomagnetic field, we find that the sustained heating model can predict perturbations that are consistent with reported experimental observations. Modifications in the quiescent heating of the lower ionosphere by thundercloud fields by individual lightning flashes may thus account for some observations of early/fast VLF events.

Plain Language Summary Intense lightning discharges cause changes to the lower ionosphere, the charged layer of the atmosphere beginning at 85 km altitude. These changes have been attributed to a number of physical mechanisms in the past two decades. In this work, we investigate the possibility that the ionosphere is held in a continuous state of heating by the presence of thunderstorms; the sudden disturbances that we measure are then caused by changes in the electrical configuration of the thunderstorm, resulting in changes to the state of heating. We investigate this proposed mechanism through modeling of thunderstorm electric fields and through modeling of propagation of the radio waves used to measure these disturbances. We find that the proposed mechanism is consistent with the data. This result was previously not possible because prior models did not consider the tilt of Earth’s magnetic field, which has a significant effect on the ionospheric heating.

1. Introduction

Thunderstorms and lightning are known to cause perturbations to subionospheric VLF transmitter signals through direct heating and ionization of the lower ionosphere; these events are broadly known as “early VLF” perturbations or events [e.g., *Armstrong*, 1983; *Inan et al.*, 1995]. The better known “early/fast” events, where the perturbation amplitude reaches its maximum within ~20 ms, have recently been joined by “early/slow” events, whose perturbation amplitude can take up to 1–2 s to reach maximum [*Haldoupis et al.*, 2006]. Early VLF events are clearly due to scattering from regions of modified conductivity in the upper atmosphere/lower ionosphere below ~90 km altitude; these conductivity changes can come from new ionization, modifying the ionospheric electron density, or through electron heating, modifying the electron-neutral collision frequency.

Despite decades of study, the physical mechanism(s) responsible for early VLF events are still under debate. *Marshall et al.* [2008] listed the candidate physical mechanisms identified to date. These include (i) scattering from ionization patches created by the quasi-electrostatic (QES) field and associated with sprite halos [*Inan et al.*, 1996a; *Pasko et al.*, 1998]; (ii) scattering from ionization columns manifested in sprites [*Dowden et al.*, 1994]; (iii) scattering from ionization associated with the lightning electromagnetic pulse (EMP) and thus elves [*Mika et al.*, 2006; *Marshall et al.*, 2010]; (iv) scattering from ionization produced by the combined QES and

EMP fields [Moore *et al.*, 2003]; and (v) “sustained heating” of the lower ionosphere by thunderstorms below [Inan *et al.*, 1996b, hereafter IPB96]. Possibilities (i)–(iv) have received the most attention and scrutiny because they involve ionization changes, the theoretical recovery times of which generally agree with early VLF event recoveries of ~ 10 – 100 s [Haldoupis *et al.*, 2009].

Modeling of EMP signals along with the observations of early/fast events and elves indicate a very weak and mostly nonexistent relationship between lightning-generated EMP signals and early/fast events [e.g., Mika *et al.*, 2006; Marshall *et al.*, 2008]. Even very large EMP events, which produce elves, have been shown to produce ionization that modifies the lower ionosphere by only 1–2%, which also have recovery times inconsistent with early/fast events. The QES fields have been linked to early/fast events with more success in explaining the observations. However, numerous observations of early/fast events with no associated sprite or halo events [Marshall *et al.*, 2006] hint at a mechanism other than electron ionization as the source of ionospheric disturbances associated with early/fast events. Furthermore, the observations of the early/fast events all indicate a vast range of recovery times of the transmitter signal [Inan *et al.*, 1993, 1996c] which is not consistent with the relaxation time scales of the electron density changes from the sprites and halos, even if one takes into account the most extreme ionospheric background and sprite-generated electron density profiles.

Recent work studying the recovery times of early VLF events has vastly increased our understanding of the physical mechanisms of the *D* region ionosphere recovery following these events [Haldoupis *et al.*, 2009; Kotovsky and Moore, 2015, 2016], in particular, the interpretation of early/slow VLF events [Haldoupis *et al.*, 2006]. Kotovsky and Moore [2015] showed that early/fast and early/slow events may in many cases be caused by the same physical mechanism but reflect different onset times in VLF data due to the interpretation of amplitude and phase data. Analysis of the scattered field phasor, on the other hand, reflects the true onset and recovery times.

In the sustained heating model, charge distributions in the thunderstorm below create electrostatic fields that reach as high as the lower ionosphere, modifying the electron temperature and thus collision frequency in a region ~ 100 km across. When a lightning discharge occurs, the charge distribution is suddenly modified, and the electrostatic fields respond immediately. This incremental change in the electrostatic field puts the lower ionosphere in a new modified state, and the VLF transmitter signal responds to this modified waveguide condition. The recovery of the early/fast VLF event, then, is reflective of the recharging of the thunderstorm below back to its predischARGE state and is controlled by the electrification processes inside the thundercloud which can have various time scales ranging from a few seconds to minutes proportional to cloud convective activity [Jacobson and Krider, 1976; Deaver and Krider, 1991; Zoghzoghy *et al.*, 2013]. IPB96 show a clear similarity between these recoveries from two separate measurements, but a direct correlation between an early/fast VLF recovery and the thunderstorm charge state has not yet been made.

The sustained heating mechanism has, to some degree, been “ruled out” because IPB96 were only able to reproduce early/fast VLF perturbations of ≤ 0.1 dB using charge moments of 100–200 C km. In contrast, early/fast VLF observations are typically 0.2–1 dB and sometimes higher. Larger charge moments result in ionization changes in the lower ionosphere, in which case the observed perturbation would be affected by the sustained heating as well as the QES and/or EMP mechanisms described above. Nonetheless, early/fast VLF events do exist for small lightning discharges, as measured by peak current [e.g., Inan *et al.*, 1993; Marshall *et al.*, 2006] which clearly cannot create electron ionization events.

In this paper, we revisit the sustained heating mechanism using a new 3-D quasi-electrostatic field model that takes into account the Earth’s magnetic field [Kabirzadeh *et al.*, 2015], which was neglected in IPB96. We show that perturbations are small, similar to IPB96, for vertical magnetic fields, but for lower dip angles the perturbations are significantly larger and may account for many early/fast events measured in the 0.2–1 dB range.

2. Modeling

2.1. Three-Dimensional Quasi-Electrostatic Field Modeling

To calculate the thundercloud electric fields which lead to the ionospheric heating, we use the 3-D model developed by Kabirzadeh *et al.* [2015]. The self-consistent solution of the fields and conductivity modifications are calculated by iteratively solving the charge conservation equation:

$$\nabla \cdot (\hat{\sigma} \nabla \Phi) = -\rho_s \sigma_{\parallel} / \epsilon_0 \quad (1)$$

where ρ_s , ϵ_0 , and Φ are thundercloud charge density, permittivity of free space, and electrostatic potential, respectively, and $\hat{\sigma}$ is the three-dimensional conductivity tensor for a magnetized plasma defined for a magnetic field in the y - z plane as follows:

$$\hat{\sigma} = \begin{pmatrix} \sigma_p & \sigma_H S & \sigma_H C \\ -\sigma_H S & \sigma_p S^2 + \sigma_{\parallel} C^2 & (\sigma_p - \sigma_{\parallel}) SC \\ -\sigma_H C & (\sigma_p - \sigma_{\parallel}) SC & \sigma_p C^2 + \sigma_{\parallel} S^2 \end{pmatrix} \quad (2)$$

where σ_{\parallel} , σ_p , σ_H are parallel, Pedersen, and Hall conductivities, respectively; $S = \sin(I)$; $C = \cos(I)$; and I is the magnetic dip angle, i.e., the angle between the magnetic field and \hat{y} . The contributions from both ion and electron conductivities are considered. The ion conductivity is obtained from previous experimental studies of the lower ionosphere [Hale, 1984]. The electron conductivity is initialized from basic equations with a given electron density profile and then solved self-consistently in the model. The effect of electron conductivity changes due to nonlinear changes of electron collision frequency with electric field is calculated using Boltzmann solvers similar to Taranenko [1993] and Pasko *et al.* [1997].

The screening charges are calculated self-consistently from the electric fields via the Poisson's equation, $\rho = -\epsilon_0 \nabla^2 \Phi - \rho_s$, at each iteration which overall reduce the "effective" charge of the thunderstorm and thus reduce the electric fields at ionospheric altitudes. The model uses a cartesian coordinate system with a nonuniform grid that has higher resolution closer to the center of the charge distributions. The side boundaries are located at 300 km away from the charges, and the top boundary is chosen at 200 km altitude above the ground.

While 2-D models either neglect the geomagnetic field or must assume a vertical field, the 3-D model of Kabirzadeh *et al.* [2015] takes into account the geomagnetic field dip angle and its strength for different latitudes and altitudes. This is an important improvement compared to the previous models of thundercloud-ionosphere electrostatic interaction [Pasko *et al.*, 1998]; for altitudes above ~ 70 km the electron gyrofrequency is larger than its collision frequency and the ionosphere behaves as a magnetized plasma [Dejnakarintra and Park, 1974; Pasko *et al.*, 1997]. Kabirzadeh *et al.* [2015] showed that for a nonvertical geomagnetic field (nonpolar latitudes) the electric fields at altitudes higher than ~ 70 km are larger than previously thought. These larger electric fields will change the electron mobilities nonlinearly and thus can significantly heat the ionosphere at middle and low latitudes.

The model neglects any electron density modifications for two reasons. First, the purpose of this paper is to estimate the thundercloud E -field-driven electron heating effects and contributions to VLF transmitter signal perturbations and thus estimate the efficiency of the heating alone as the mechanism responsible for early/fast events. Second, the chemical reaction processes (ionization and attachment) require considerably larger electric fields, similar to the transient fields generated by lightning, which are not available during the thundercloud charging time and after the lightning transient fields and their effects have terminated. Here we are interested in the ionospheric equilibrium state before and after the lightning discharge. We have restricted the charge moment changes used in this work to values insufficient to produce new ionization and confirmed the absence of new ionization in the model outputs.

Furthermore, the convective motion of ionospheric electrons due to the radial component of the electric fields might also change the electron density configuration. The effectiveness and relevance of these effects are nevertheless beyond the scope of this paper and require further investigation.

2.2. Propagation Modeling

To estimate the VLF subionospheric signal perturbation resulting from these thundercloud fields and heating of the ionosphere, we use a 2-D Finite-Difference Time-Domain (FDTD) model as described in detail by Marshall [2012], which we refer to as the Electromagnetic Pulse (EMP) model.

The EMP model solves Maxwell's equations in a cold, collisional, magnetized plasma, using the Lee and Kalluri algorithm [Lee and Kalluri, 1999] to solve the auxiliary plasma equation. The model solves for all six field components plus three components of the current J in the Earth-ionosphere waveguide and in the lower ionosphere with high spatial resolution over propagation distances of thousands of kilometers. The model is cast in spherical coordinates, so that it naturally accounts for the curvature of the Earth and the decay of the propagating fields as they expand in the waveguide. The model can take arbitrary electron density, collision frequency, and background magnetic field profiles that can vary over the 2-D simulation space, as well as ground and ionospheric parameters (conductivity and permittivity) that vary along the 1-D propagation path.

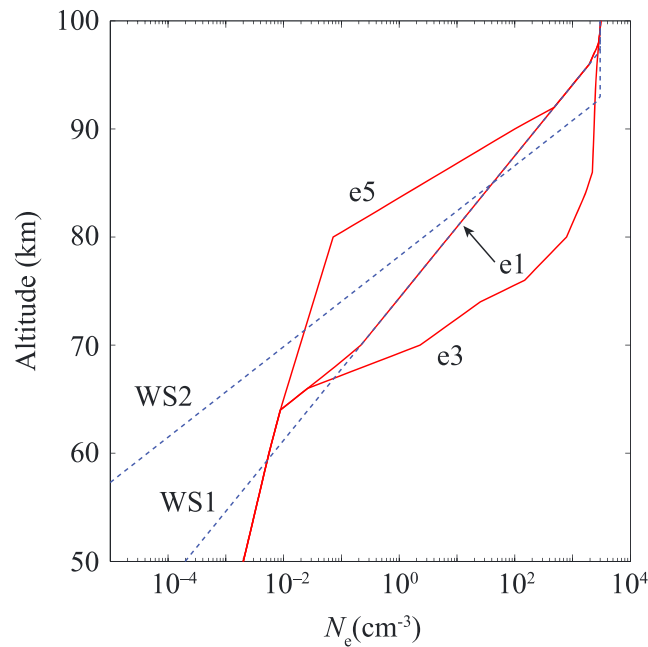


Figure 1. Ionospheric electron density profiles used in this study. Profiles e1, e3, and e5 are identical to those used in prior published work; WS1 and WS2 are two different Wait and Spies profiles, using $\beta = 0.5$ and 0.7 , with $h' = 85$ km for both. Note that e1 and WS1 are identical in the region where VLF reflection occurs (~ 70 – 90 km).

The method uses a convolutional perfectly matched layer (PML) absorbing boundary Roden and Gedney [2000] above the ionosphere and at the far end of the simulation path. For its use in VLF transmitter subionospheric propagation, this model has recently been validated against the LWPC model and another Finite-Difference Frequency Domain (FDFD) model [Marshall et al., 2016], showing excellent agreement for both absolute amplitude and phase, as well as the magnitude of perturbations for a given ionospheric disturbance.

The EMP model simulates the electromagnetic wave propagation resulting from an impulsive, broadband source similar to a lightning discharge, with bandwidth from DC to 400 kHz. To simulate VLF transmitters, we compute discrete Fourier transforms (DFTs) at every point along the ground and at preselected frequencies of interest:

$$\mathcal{E}_z(x, z, \omega_0) = \sum_{n=1}^N E_z(x, z, n) e^{i\omega_0 n \Delta t} \Delta t \quad (3)$$

where ω_0 is the frequency of interest, Δt is the time step in the simulation, and $E_z(x, z, n)$ is the vertical component of the electric field at altitude z , range x , and time step n . One requirement of this method is that the DFT is computed long enough (N total time steps) so that the fields have settled at the locations of interest; in practice we determine this duration N through numerical experiments. From these DFTs, the amplitude and phase at each frequency can be easily extracted. The FDTD method has the advantage that a large number of frequencies can be computed simultaneously, with very little addition to the computation time of the simulation.

For this paper, we solve for subionospheric VLF waves propagating over ~ 2500 km horizontal distance (x) and up to 110 km altitude (z), which is well above the reflection altitude of the transmitter signal (~ 85 km). The solutions are found on a spatial grid with $\Delta x = \Delta z = 0.5$ km. We use a simulation path (i.e., ground parameters) from the NAA transmitter in Cutler, Maine, to a receiver in Colorado, to emulate many of the early VLF events observed in the 1990s and 2000s by the Holographic Array for Ionospheric Lightning (HAIL) array [Johnson and Inan, 2000]. The modified electron collision frequency found from the 3-D QES model is inserted into the FDTD model ~ 1200 km from the transmitter. This distance places the disturbance beyond most of the prominent interference nulls in amplitude but provides enough distance between the disturbance and receiver to estimate a statistically significant expected perturbation magnitude.

To solve for the perturbation amplitude and phase changes, we run the EMP model twice: once with the 2-D collision frequency profiles resulting from the dipole field distribution computed by the QES model and then again with the collision frequencies determined by the monopole field distribution. The difference in the amplitude and phase for these two simulations gives us an estimate of the perturbation that would result from the removal of the upper charge layer in the dipole configuration, after transients have settled.

2.3. Ionosphere Profiles

To take into account ionospheric variability, we consider five different electron density profiles, shown in Figure 1. Profiles e1, e3, and e5 are taken from previous studies of subionospheric VLF transmission [Pasko and Inan, 1994; Pasko et al., 1998] and used here for historical continuity. They represent canonical nighttime electron density profiles that are average, dense, and tenuous, respectively. The WS1 and WS2 profiles are from

theoretical studies of the ionosphere [Wait and Spies, 1964] with the VLF reflection height $h' = 85$ km and the “steepness” parameter $\beta = 0.5$ and 0.7 km^{-1} for WS1 and WS2, respectively. The range of values here agree with assessments using VLF remote sensing [Thomson et al., 2007] and lightning sky wave analysis [Lay et al., 2014]. These profiles provide a range of nighttime ionospheres to explore the penetration of electrostatic fields. We note that profiles e5 and WS2 are the most tenuous below 85 km, and so we expect the strongest field penetration to *D* region altitudes for these profiles. We note also that profiles e1 and WS1 are very similar above 70 km, and so we expect similar results with those two profiles.

3. Results

3.1. Electrostatic Heating Results

For the 3-D QES model, we begin with a dipole charge distribution, with a positive point charge placed at an upper altitude and a negative point charge placed at a lower altitude. Inan et al. [1996b] used charge centers at 10 and 20 km, with charge removed from 20 km, to explore the upper bounds of realistic scenarios. In this work, we use charge centers at 5 and 10 km to simulate a more common scenario. In section 3.4 we will explore the effects of charge centers at different altitudes. Since the purpose of this work is to study the effects of heating alone, we have ensured that all simulations do not produce any electron density changes. Charge moment changes (ΔM_q) of 400 C km or higher do produce electric fields strong enough to exceed the threshold for dissociative attachment, but not strong enough to exceed the breakdown threshold (and thus produce ionization). However, the inclusion of associative detachment nulls the effect of attachment by detaching those lost electrons from O^- very quickly [Liu, 2012]. We observe that the electron density change due to this ΔM_q only persists for a few milliseconds.

We solve for the electrostatic fields in steady state using the QES model. Then, we repeat the model calculation after having removed the positive charge from the upper altitude. For example, if we place -20 C at 5 km altitude and $+20 \text{ C}$ at 10 km altitude and then remove the upper charge, we are inducing a charge moment change ΔM_q of 200 C km. These calculations result in two different 3-D profiles of modified collision frequency, for the dipole and monopole configurations, 2-D slices of which are then input into the propagation model.

Similarly, two simulations are computed using the EMP model, first using the collision frequency associated with the dipole charge and second with the monopole charge. The difference between the resulting propagation simulation outputs yields the VLF perturbation magnitude in both amplitude and phase along the ground.

Figure 2 shows simulation results for charge centers of 20 C at 5 and 10 km altitude. The color plots show 2-D slices of the 3-D simulations, showing the percent change in collision frequency after removing the positive upper charge region. These simulations suggest a significant heating effect, with the effective collision frequency changing by as much as 70% at lower *D* region altitudes where the VLF transmitter signal reflects.

We can observe a few trends from these simulations. First, Figure 2 (top row) shows that the heating extends to higher altitudes for lower dip angles, i.e., horizontal magnetic field, near the equator. Figure 2 (bottom row), showing results for different ionospheres, shows that the more tenuous ionospheres (e5 and WS2) show more prominent heating and extend to higher altitudes, as expected. The dense e1, e3, and WS1 ionospheres do not allow the electrostatic fields to penetrate above ~ 75 km altitude.

To help quantify the heating effect, Figure 3 shows 1-D slices through the center of the heating region, at altitudes of 70, 75, and 80 km. These slices show the absolute value of the peak heating disturbance as change in collision frequency, reaching above 70% in some cases, as well as the spatial extent, covering ~ 50 km half width at half maximum (HWHM) or larger in almost all cases. This spatial extent is very consistent with the disturbance regions reported by Johnson and Inan [2000], having a radius of 50 km based on measured early/fast VLF perturbations.

3.2. Propagation Modeling Results

Next, the 2-D slices of the disturbed ionosphere are inserted into the EMP model to simulate the perturbed signal at a VLF receiver. We run the EMP model with ionospheric collision frequency disturbances corresponding to heating due to the monopole electric field and with heating due to the dipole electric field. The results in this paper show the difference between the dipole and monopole cases, to simulate the change in amplitude and phase that would be measured when the upper charge region is suddenly removed.

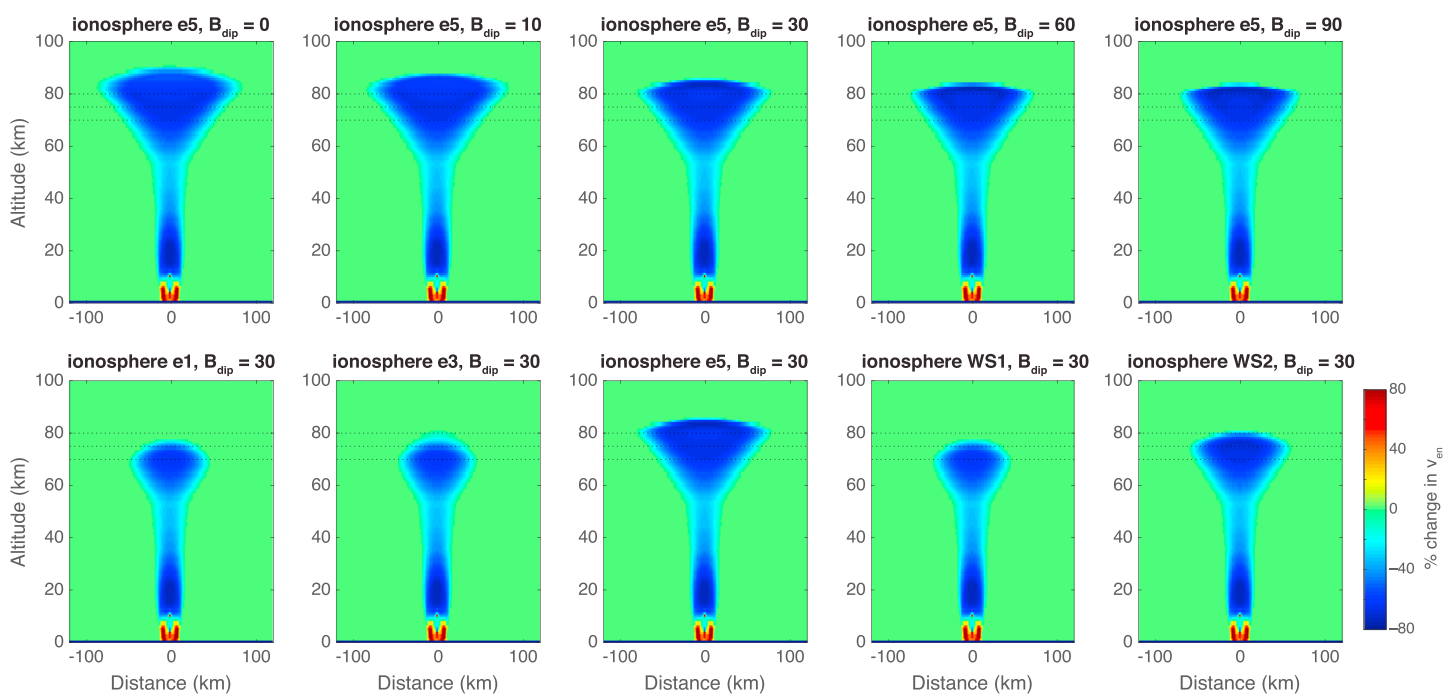


Figure 2. Two-dimensional slides through the 3-D simulation volume for the QES model outputs, for ± 40 C charge centers at 5 and 10 km altitude. These plots show the change in collision frequency, between monopole and dipole field cases; i.e., the upper 40 C has been removed from 10 km altitude. (top row) Different magnetic dip angles, using the same ionosphere e5; (bottom row) different ionospheres with a consistent dip angle.

We use an impulsive source in the EMP model with bandwidth from DC to 60 kHz. For the present work, we extract the amplitude and phase at frequencies from 16 to 30 kHz, and here we will show results at 20 kHz, similar to VLF transmitters operating in the U.S. and Europe. We have also compared the outputs for 24 kHz (not shown), corresponding to the NAA transmitter; these results show perturbations with very similar magnitudes. Figure 4 shows an example of the amplitude (top) and phase (bottom) at 20 kHz extracted from the EMP model, for an e1 ionosphere simulation. Nulls are observed in the amplitude plot at distances of ~ 300 and ~ 500 km and a very shallow null at ~ 1300 km; in the phase signal, the prominent nulls are manifested as sudden jumps in phase.

Figure 5 shows the amplitude and phase, as well as amplitude and phase perturbations, for the simulated cases with 40 C charge removed from 10 km altitude. Note that the phase shown is the phase residual, i.e., the deviation from the expected phase based on speed of light propagation along the ground. The 25 total simulations are for different combinations of five ionospheres and five magnetic field dip angles. Nulls have been removed using an empirical metric where we search for rapid changes in amplitude (dA/dx) above some estimated threshold and remove a 50 km region of amplitude and phase. We use a threshold of 0.4 dB/km, determined by trial and error, to remove nulls; we have tested thresholds from 0.2 to 0.5 dB/km and find that the results described later in this paper are unaffected. The results in Figure 5 demonstrate that nulls have been removed from the amplitude and phase plots, so that artificially high perturbations near these nulls are not considered in the analysis and statistics shown in this paper.

Recall that the heated ionosphere disturbance is placed at 1200 km range from the transmitter; we observe that amplitude and phase perturbations begin near this distance. We can see from Figure 5 that amplitude and phase perturbations can reach as high as 0.5 dB and $\sim 3^\circ$, respectively, after removing nulls. These values correspond to above-average early/fast perturbations in narrowband VLF data but not extreme values.

Figure 6 summarizes the statistics of the simulated perturbations with 400 C km charge moment change. Note that the results for the WS1 ionosphere are not shown, as they are identical to the results for the e1 ionosphere. For each simulation, we measure the perturbation as a distribution of amplitude and phase change along the path from 1300 to 2200 km from the transmitter. In each panel, the solid blue line shows the median perturbation, and the shaded region bounds the 10% and 90% percentiles; that is, of the possible perturbation values measured between 1300 and 2200 km, the central 80% will fall in this shaded region.

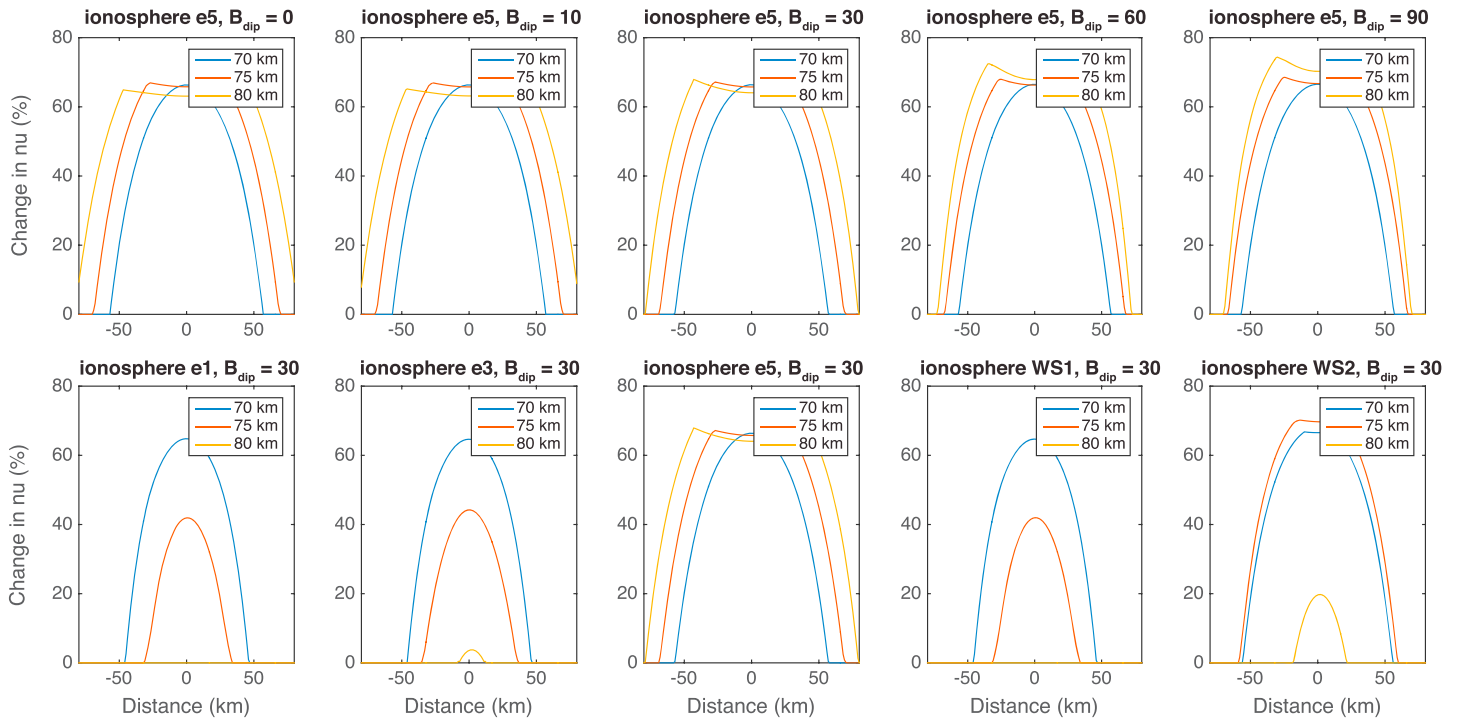


Figure 3. One-dimensional slides through the 2-D disturbances from Figure 2, at 70, 75, and 80 km altitude, showing absolute value of Δv_{en} . These slices demonstrate a disturbance HWHM of ~ 50 km, depending on the ionosphere and magnetic field parameters.

We observe that amplitude perturbations fall within the range of measurable values for the e5 and WS2 ionospheres. Values for the e1 ionosphere are at the edge of detectability, and values for the e3 ionosphere are far below measurable, where most receivers do not observe perturbations below ~ 0.1 dB or 0.5° of phase change. Furthermore, the major contribution of the 3-D QES model is manifested in the trends for each plot: larger perturbations are observed for near-horizontal magnetic fields. For example, for the e5 ionosphere, where a typical perturbation of only 0.02 dB would be observed for a vertical magnetic field, the perturbation rises to 0.1–0.3 dB for a horizontal magnetic field, well within the observable range. This result provides support for

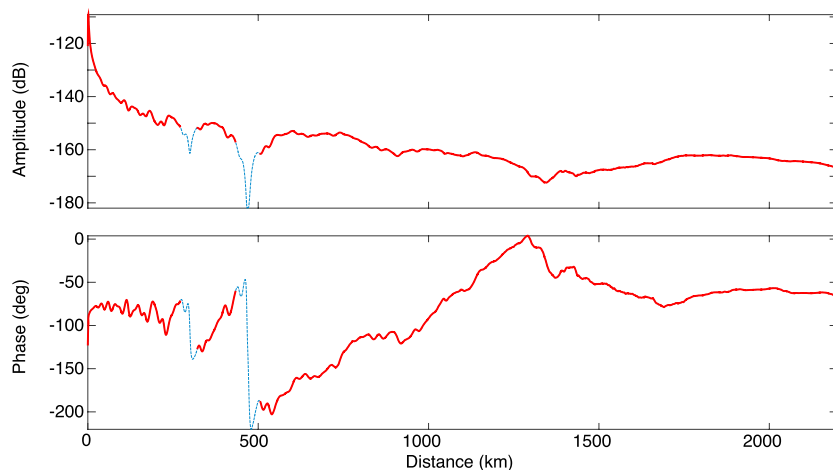


Figure 4. Example output of the FDTD model. (top) Relative amplitude extracted along the ground at 20 kHz. (bottom) Phase extracted along the ground at 20 kHz and unwrapped. Nulls such as the one at ~ 500 km are removed before processing amplitude and phase changes due to heating disturbances; the thin blue dashed line shows where nulls have been removed. In this case, the shallow null near ~ 1300 km was not removed since it does not include a sudden phase jump.

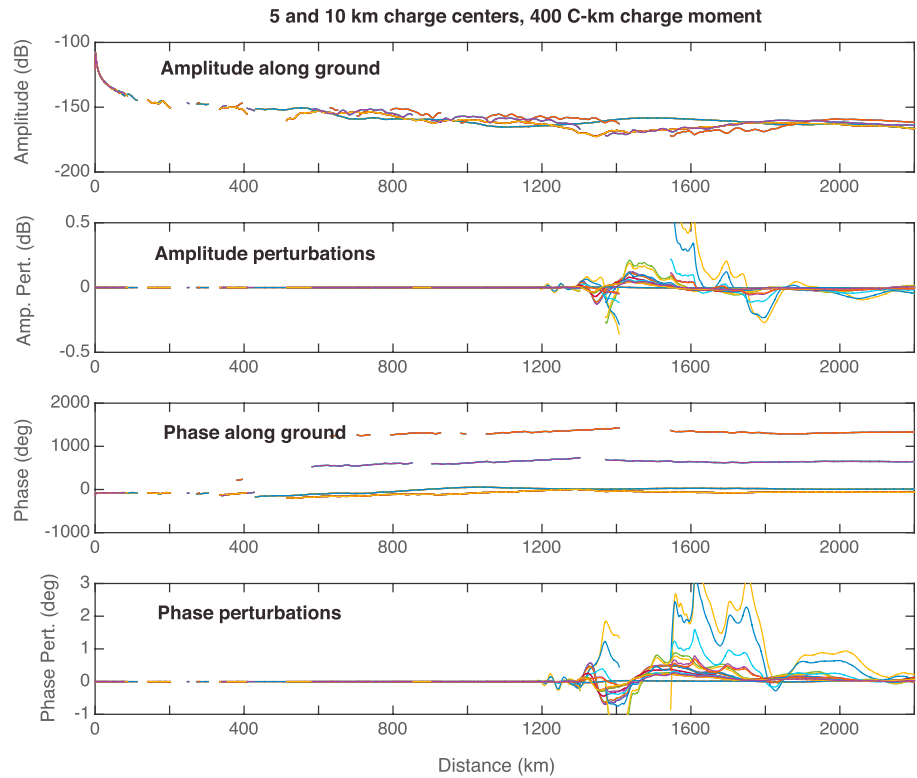


Figure 5. Amplitude and phase versus distance for simulations through different ionospheres and different heating disturbances. (first panel) Amplitude for each simulation; nulls have been cut out using an empirical metric as described in the text. (second panel) Amplitude perturbations due to the removal of the upper charge layer. (third panel) Phase along the ground for different scenarios and (fourth panel) phase disturbances due to removal of upper charge layer.

the sustained heating mechanism to produce early VLF events and shows that such events are more likely for low magnetic dip angles (i.e., low latitudes).

3.3. Charge Moment Change Dependence

In this section we explore the effect of the charge moment change on expected amplitude and phase perturbations. Figure 7 shows perturbation statistics similar to Figure 6, but for a ΔM_q of 200 C km; i.e., 20 C charge centers at 5 and 10 km, with the upper charge removed. Comparing the two figures, we can observe that many of the same trends hold true, such as the magnetic dip angle dependence and the response of different ionospheres. The magnitude of observed perturbations is considerably less: about half in the case of the

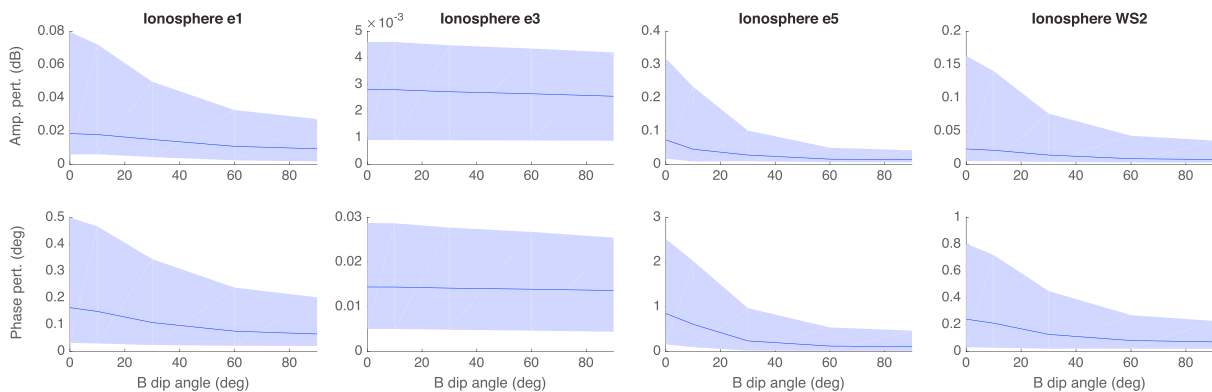


Figure 6. (top row) Amplitude and (bottom row) phase perturbations for different ionospheres as a function of dip angle, for 40 C charge centers at 5 and 10 km, after the 10 km charge is removed. The solid line shows the median perturbation between 1300 and 2200 km from the transmitter; the shaded region bounds the 10% and 90% percentiles.

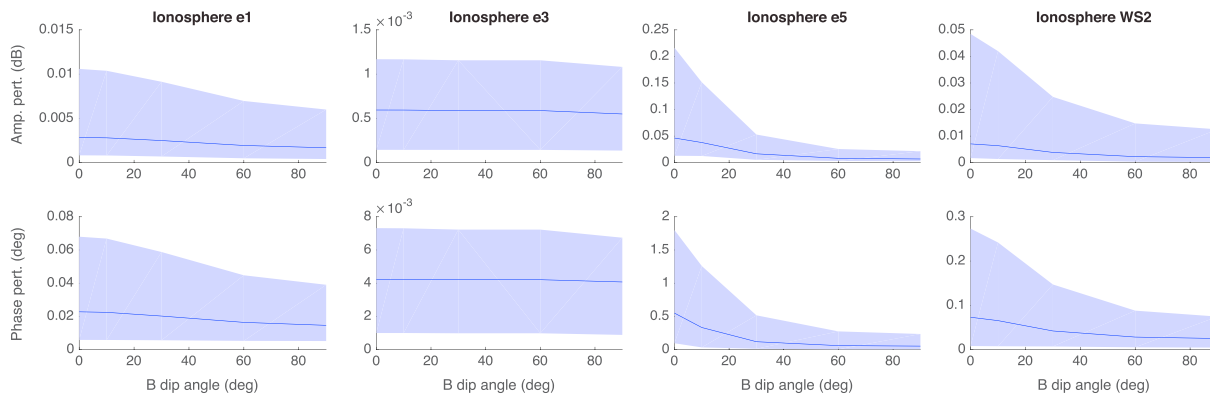


Figure 7. Same as Figure 6, but for a 200 C km ΔM_q from 10 km altitude. We observe that the amplitude and phase perturbations are weaker than the previous case by about a factor of 2, although the increase varies for each ionosphere.

e5 ionosphere but significantly less for the other ionospheres. The heating effect is known to be a nonlinear function of the reduced electric field, so we expect that while halving the ΔM_q will halve the magnitude of the electric field, the resulting heating will be significantly less than half.

Next, for charge centers at 5 and 10 km, we vary the ΔM_q to investigate the trend in the heating and VLF perturbations with increasing ΔM_q . We investigate ΔM_q from 100 C km (10 C at 10 km) up to 600 C km (60 C at 10 km). The latter is used as an upper limit, above which ionization is likely to occur at mesospheric altitudes. Indeed, *Cummer and Lyons [2005]* have shown that sprites are produced with an increasing probability for ΔM_q above 600 C km, but the vast majority of ΔM_q below 600 C km do not produce sprites, implying that at about 600 C km, the field approaches the breakdown threshold and is intense enough to induce ionization.

Figure 8 shows the disturbed collision frequency profiles, in 2-D slides, for ΔM_q varying from 100 C km to 600 C km. For this part of the study we use the WS2 ionosphere profile and a magnetic dip angle of 30°, as this ionosphere and magnetic dip angle lie in between the extremes of our range of inputs. The heating signatures show increasing effects with increasing ΔM_q , as expected, and the effects appear to be nonlinear with ΔM_q . However, the 1-D slices in the third row, showing the absolute value of the peak heating disturbance, show an interesting and unexpected effect. At 75 km altitude, for example, the peak change in collision frequency appears to saturate above ~300 C km; however, the width of the disturbed region continues to increase. Nonetheless, at 80 km altitude, the heating does increase with larger charge moment changes, implying that the field can penetrate to higher altitudes with larger ΔM_q .

Figure 9 shows the results of EMP simulations using the heated ionospheres used to produce Figure 8. Figure 9 (left column) shows the amplitude and phase perturbations along the ground for each ΔM_q scenario; Figure 9 (middle and right) show the perturbation trends with ΔM_q . Again, the solid line shows the median perturbation, and the shaded region bounds the 10% to 90% percentiles of perturbations that would be measured between 1300 and 2200 km range. Nulls have been removed using the same criteria as earlier; a large null has been removed between 1300 and 1400 km range. The perturbation magnitudes appear to increase close to linearly with ΔM_q .

For relatively large $\Delta M_q = 600$ C km, the maximum perturbations in amplitude and phase are above the measurable values when compared to past observations. Note that this is shown in Figure 9 for the WS2 ionosphere; the e5 ionosphere shows considerably larger perturbations. These results suggest that typical charge moment changes, where charge is removed from 10 km altitude or higher, are likely to produce perturbations measurable by VLF subionospheric remote sensing. Discharges from lower altitudes, or with lower charge moment changes, may not produce measurable perturbations.

3.4. Altitude Dependence

Finally, we investigate the effects of the altitude of charge centers on these perturbation magnitudes. QES and EMP simulations were conducted with 10 C charge centers under the following scenarios: (i) lower charge at 5 km altitude and upper charge at altitudes from 12 to 20 km in 2 km steps, and (ii) lower charge at 10 km altitude and upper charge at altitudes from 12 to 20 km in 2 km steps. All of the presented simulations use the

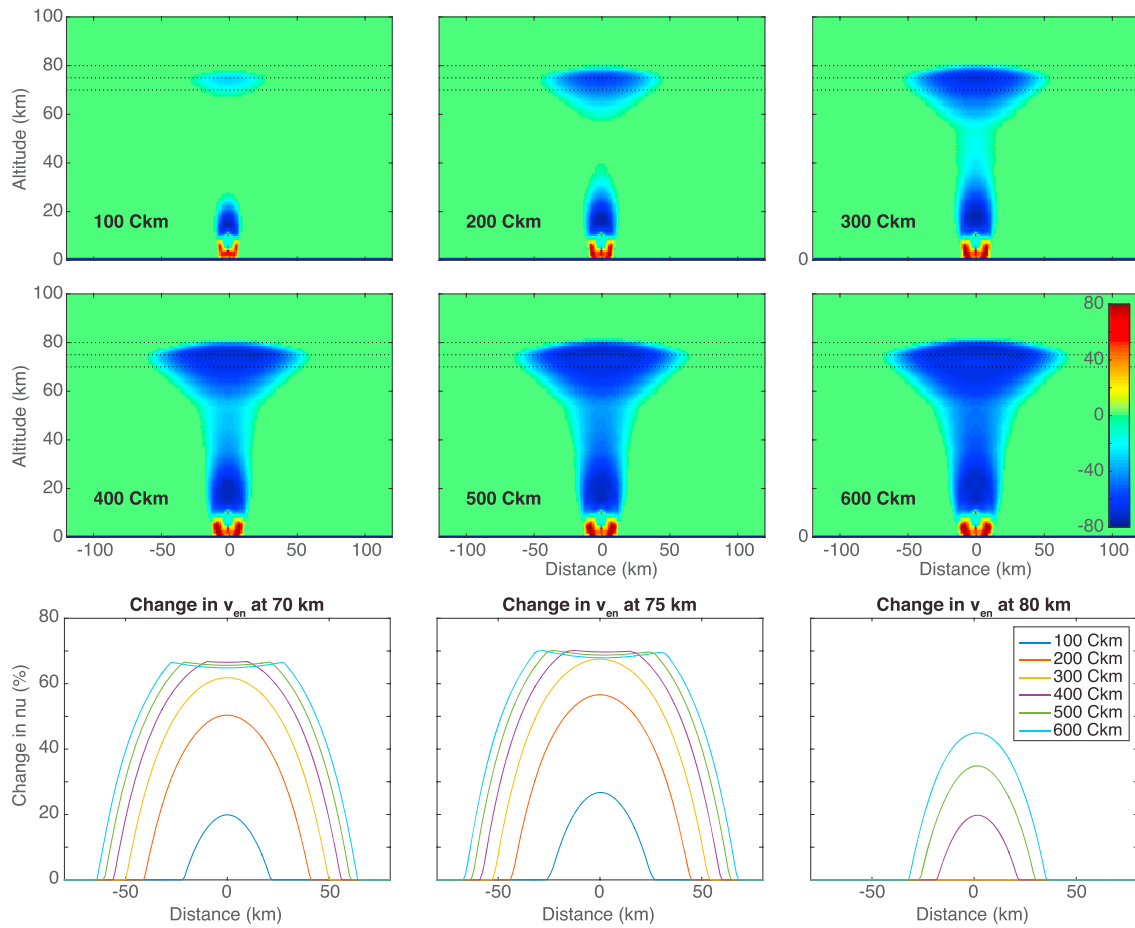


Figure 8. Collision frequency disturbances for increasing ΔM_q , with charge centers at 5 and 10 km. (first and second rows) Differences in collision frequency profiles between dipole and monopole configurations. (third row) Horizontal slices of the absolute value of Δv_{en} through 70, 75, and 80 km altitudes. These simulations use the WS2 ionosphere profile and a magnetic dip angle of 30° .

WS2 ionosphere and a magnetic dip angle of 30° as before. The resulting perturbation statistics are shown in Figure 10. Comparing the left and right columns, where the lower charge altitude is changed, we observe that the lower charge altitude has only a weak effect on the resulting perturbations. On the other hand, increasing the upper charge altitude increases the perturbation magnitudes in both amplitude and phase, with a nonlinear increase.

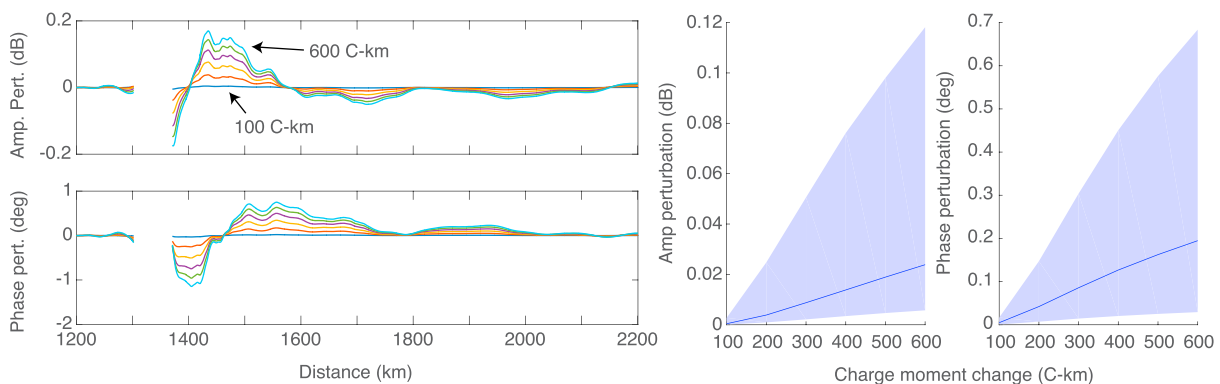


Figure 9. VLF perturbations at 20 kHz for increasing ΔM_q . (left column) The amplitude (top) and phase perturbation (bottom) along the ground for each case; (middle and right) the median perturbation magnitudes as a function of ΔM_q , with shading representing the 10% to 90% ranges.

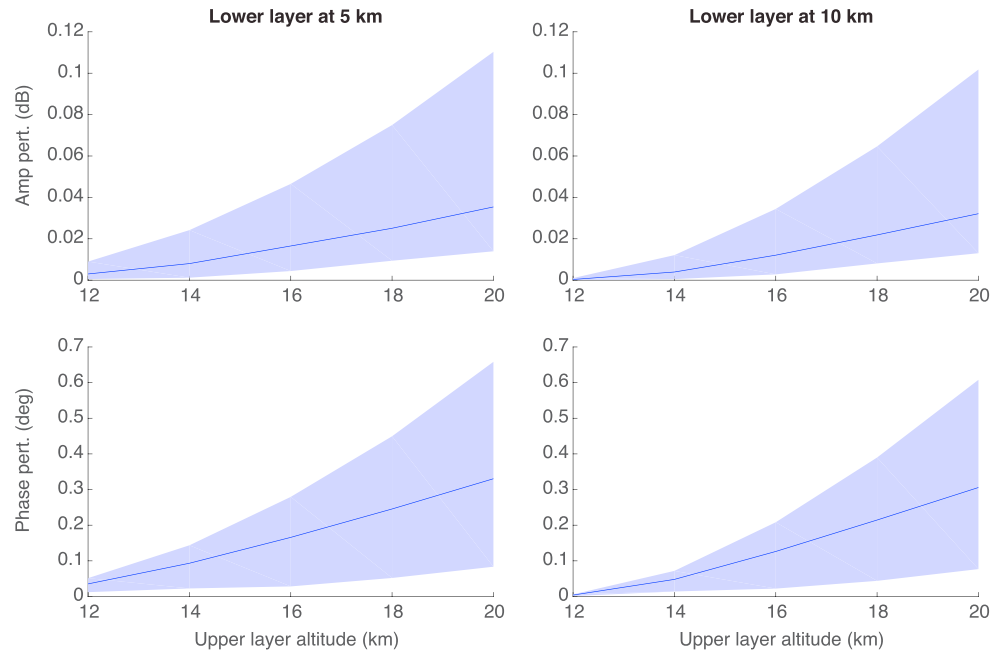


Figure 10. VLF perturbations at 20 kHz for increasing ΔM_q . (left column) The amplitude and phase perturbation along the ground for each case; (right column) the median perturbation magnitudes as a function of ΔM_q , with shading representing the 10% to 90% percentiles. These simulations use the WS2 ionosphere profile and a magnetic dip angle of 30° .

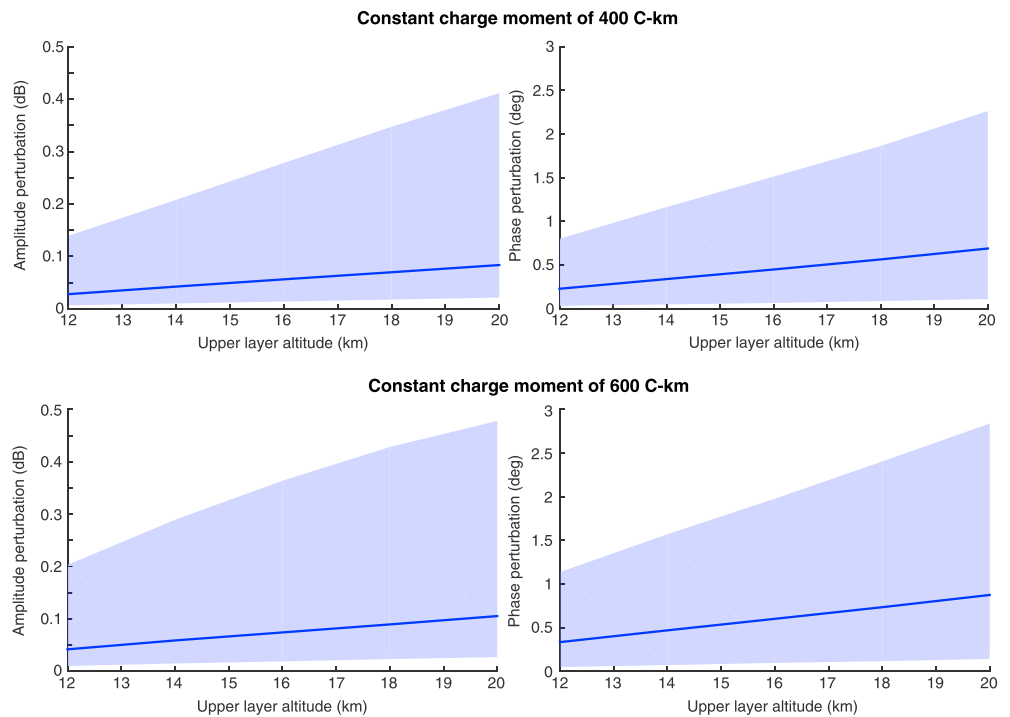


Figure 11. Magnitudes of VLF perturbations at 20 kHz for a constant charge moment change, but the altitude of the upper charge layer (and thus the magnitude of both charge layers) is varied to maintain constant ΔM_q . (top row) Amplitude and phase for $\Delta M_q = 400$ C km; (bottom row) amplitude and phase for $\Delta M_q = 600$ C km.

It is important to note that since the altitude of the upper charge layer is increasing, the charge moment is also increasing. The 10 C removed from 12 km altitude corresponds to 120 C km, while the same charge removed from 20 km is a ΔM_q of 200 C km. However, Figure 9 demonstrated that simply increasing the charge moment, without changing the altitude, results in a nearly linear increase in perturbation magnitude. The faster-than-linear increase in perturbation magnitude in Figure 10 suggests that the altitude has a separate effect. Indeed, at higher altitude the upper charge layer is closer to the ionosphere, so we expect its field to have a larger heating effect.

It is also worth noting here that the maximum ΔM_q shown is 200 C km when the charge is removed from 20 km altitude. Even with this relatively modest ΔM_q , the perturbations reach measurable values. Larger charge moment changes from these high altitudes, or with a more receptive ionosphere such as e5, will result in much larger perturbations.

Because the same amount of charge is being removed from progressively higher altitudes, Figure 10 wraps together the effect of higher altitude with the effect of higher charge moment change. To separate the two effects, Figure 11 plots the same results, but in this case ΔM_q is held constant. The total charge removed has been varied for each altitude in order to keep ΔM_q constant at 400 C km (top row) or 600 C km (bottom row). The lower charge is placed at an altitude of 5 km in all cases. Clearly, this figure shows that the higher altitude charge center produces larger disturbances in the ionosphere and in turn larger perturbations to the subionospheric VLF signal. The mean perturbations (solid blue line) are $\sim 26\%$ larger for 600 C km compared to 400 C km, i.e., significantly larger but not proportional to the charge moment change.

4. Summary and Discussion

The results presented in the previous section demonstrate that the sustained heating mechanism of *Inan et al.* [1996b] is capable of producing a sufficiently disturbed ionosphere to be measured as an early VLF event following a large positive cloud-to-ground (+CG) discharge. However, it is clear that the mechanism produces very small perturbations that only exceed the threshold for measurement under particular circumstances. We have shown that the Earth's magnetic field dip angle is an important consideration and that the sustained heating mechanism is more likely to produce early VLF events at low latitudes. Of note, we have also simulated –CG cases, where the same charge is removed from the lower charge layer. In those cases, the perturbation magnitudes are considerably smaller and likely not measurable. Hence, this type of early VLF perturbation is likely to be primarily associated with +CGs.

We have simulated a charge moment change (ΔM_q) of 400 C km by removing 40 C of charge from 10 km altitude and lower or higher charge moment changes by using a smaller or larger charge quantity. In all cases, the quasi-electrostatic field at high altitudes is not strong enough to produce ionization, as we are interested in the effect of sustained heating only. The resulting change in ionospheric heating is strong enough to produce measurable early VLF events, especially for a tenuous nighttime ionosphere, and low magnetic dip angles. We conclude that the sustained heating mechanism is a feasible source of early VLF events for large ΔM_q and for discharges from reasonably high altitudes, while still below the ΔM_q required to produce ionization. However, the sustained heating mechanism is much less likely to produce detectable early VLF events at moderate to high magnetic dip angles, where the perturbation magnitudes are low.

An important implication of the quiescent heating model is the source of the disturbance which controls the decay rate and the duration of the early VLF event. Based on this model, the decay rate is controlled by the interplay between the charging mechanism in the thundercloud and the relaxation time of the E field at different altitudes and is not controlled by the relaxation of the ionospheric electrons due to recombination. Thus, observations of early/fast VLF events reflect the recharging rate of the thundercloud following a discharge. Confirmation of this method via experiment could be done with ground-based electric field mills (EFMs) located under the thunderstorm, and a VLF receiver located a few hundred to a thousand kilometers away, along a VLF transmitter great circle path which passes over the EFM(s). The EFMs would measure the recharging of the thundercloud, while the VLF narrowband signal would monitor the ionospheric response.

The quiescent heating model may have implications for the observations of early/slow events. *Marshall et al.* [2008] simulated the effect of up to hundreds of in-cloud lightning pulses that occurred on the lower ionosphere and argued that early/slow events can be explained as the cumulative result of many in-cloud lightning

electromagnetic pulses creating a density hole through dissociative attachment at lower ionospheric altitudes. Alternatively, the quiescent heating model can explain observations as the repetitive redistribution and removal of the thundercloud charge density which can change the ionospheric heating level. This result is consistent with observations of lightning activity associated with early/slow VLF events. As was noted by Haldoupis *et al.* [2006], lightning activity associated with early/slow events usually consists of a postonset sequence of CG discharges coming from the same area and a large number of weaker but densely clustered sferics which are most likely in-cloud (IC) pulses in the same area. The subsequent CGs and the in-cloud activity can each contribute to the modification of charge distribution and thus ionospheric heating which leads to the gradual change in the VLF transmitter signal amplitude and/or phase. The rise time of the signal is thus associated with the time span of the burst of lightning activity. The existence of some "pre-early" events where the VLF events start even before the causative CG lightning [Haldoupis *et al.*, 2006] suggests that the electron density disturbances associated with sprite halos were not the cause of the VLF perturbations; rather, the in-cloud activity prior to the CG caused changes in the ionospheric conditions through the quiescent heating mechanism. The quiescent heating model is thus an alternative to the EMP model of Marshall *et al.* [2008] as an explanation for the production of early/slow events.

Kotovskiy and Moore [2015] showed that early/fast and early/slow events may be caused by the same physical mechanism but may be interpreted differently simply due to the analysis of VLF amplitude and phase data. Early VLF events caused by the sustained heating mechanism here need to be analyzed accordingly to accurately determine the onset time.

There has been a question of the frequency of the observations of early VLF events based on the predictions of the quiescent heating model [Haldoupis *et al.*, 2006]. We have shown in this paper that the VLF signal amplitude and phase change observed at a receiver depends on the receiver location behind the disturbance. The largest signal perturbations are predicted when the lightning-associated heating of the lower ionosphere lies on the great circle path between the transmitter and the receiver. However, even for this case the relationship between the received signal perturbation and the distance between the receiver and the disturbance is rather complicated. Thus, large ionospheric disturbances might result in a negligible received signal perturbation, below the detectable level of the receiver, that are left undetected. Moreover, the ionospheric electron density profile and the geomagnetic dip angle can greatly impact the effectiveness of the thunderclouds on influencing the VLF transmitter signals.

We conclude that the quiescent heating mechanism may account for the production of some early VLF events, but most events are likely produced by electron density changes associated with the quasi-electrostatic field. It is very likely that during strong cloud-to-ground lightning, a combination of the electron density changes and electron heating mechanisms contribute to observed early VLF events. The quiescent heating model, therefore, is consistent with observations of sprites in association with early VLF events [Haldoupis *et al.*, 2004; Mika *et al.*, 2005] as well as observations of these events not associated with sprites [Marshall *et al.*, 2006].

Acknowledgments

This work was supported by DARPA grant HR0011-10-1-0058 and NSF CEDAR grant AGS-1243176. The simulation data and analysis codes used to generate all figures and results in this paper are available at <https://github.com/ram80unit/QES-JGR-2017>.

References

- Armstrong, W. C. (1983), Recent advances from studies of the Trimp effect, *Antarct. J. USA*, 18, 281–283.
- Cummer, S. A., and W. A. Lyons (2005), Implications of lightning charge moment changes for sprite initiation, *J. Geophys. Res.*, 110, A04304, doi:10.1029/2004JA010812.
- Deaver, L. E., and E. P. Krider (1991), Electric fields and current densities under small Florida thunderstorms, *J. Geophys. Res.*, 96(D12), 22,273–22,281.
- Dejnakarintra, M., and C. Park (1974), Lightning-induced electric fields in the ionosphere, *J. Geophys. Res.*, 79(13), 1903–1909.
- Dowden, R. L., C. D. D. Adams, J. B. Brundell, and P. E. Dowden (1994), Rapid onset, rapid decay (RORD), phase and amplitude perturbations of VLF subionospheric transmissions, *J. Atmos. Terr. Phys.*, 56(11), 1513–1527.
- Haldoupis, C., T. Neubert, U. S. Inan, A. Mika, T. H. Allin, and R. A. Marshall (2004), Subionospheric early VLF signal perturbations observed in one-to-one association with sprites, *J. Geophys. Res.*, 109, A10303, doi:10.1029/2004JA010651.
- Haldoupis, C., R. J. Steiner, A. Mika, S. Shalimov, R. A. Marshall, U. S. Inan, T. Bosinger, and T. Neubert (2006), "Early/slow" events: A new category of VLF perturbations observed in relation with sprites, *J. Geophys. Res.*, 111, A11321, doi:10.1029/2006JA011960.
- Haldoupis, C., A. Mika, and S. Shalimov (2009), Modeling the relaxation of early VLF perturbations associated with transient luminous events, *J. Geophys. Res.*, 114, A00E04, doi:10.1029/2009JA014313.
- Hale, L. C. (1984), Middle atmosphere electrical structure, dynamics, and coupling, *Adv. Space Res.*, 4(4), 175–186.
- Inan, U. S., J. V. Rodriguez, and V. P. Idone (1993), VLF signatures of lightning-induced heating and ionization of the nighttime D-region, *Geophys. Res. Lett.*, 20(21), 2355–2358.
- Inan, U. S., T. F. Bell, V. P. Pasko, D. D. Sentman, E. M. Wescott, and W. A. Lyons (1995), VLF signatures of ionospheric disturbances associated with sprites, *Geophys. Res. Lett.*, 22(24), 3461–3464.
- Inan, U. S., A. Slingeland, V. P. Pasko, and J. V. Rodriguez (1996a), VLF and LF signatures of mesospheric/lower ionospheric response to lightning discharges, *J. Geophys. Res.*, 101(A3), 5219–5238.

- Inan, U. S., V. P. Pasko, and T. F. Bell (1996b), Sustained heating of the ionosphere above thunderstorms as evidenced in "early/fast" VLF events, *Geophys. Res. Lett.*, **23**(10), 1067–1070.
- Inan, U. S., W. A. Sampson, and Y. N. Taranenko (1996c), Space-time structure of optical flashes and ionization changes produced by lightning-EMP, *Geophys. Res. Lett.*, **23**(2), 133–136.
- Jacobson, E. R., and E. P. Krider (1976), Electrostatic field changes produced by Florida lightning, *J. Atmos. Sci.*, **33**(1), 103–117.
- Johnson, M. P., and U. S. Inan (2000), Sferic clusters associated with early/fast VLF events, *Geophys. Res. Lett.*, **27**(9), 1391–1394.
- Kabirzadeh, R., N. Lehtinen, and U. S. Inan (2015), Latitudinal dependence of static mesospheric *E* fields above thunderstorms, *Geophys. Res. Lett.*, **42**, 4208–4215, doi:10.1002/2015GL064042.
- Kotovsky, D. A., and R. C. Moore (2015), Classifying onset durations of early vlf events: Scattered field analysis and new insights, *J. Geophys. Res. Space Physics*, **120**, 6661–6668, doi:10.1002/2015JA021370.
- Kotovsky, D. A., and R. C. Moore (2016), Photochemical response of the nighttime mesosphere to electric field heating—Onset of electron density enhancements, *J. Geophys. Res. Space Physics*, **121**, 4782–4799, doi:10.1002/2015JA022054.
- Lay, E. H., X.-M. Shao, and A. R. Jacobson (2014), *D* region electron profiles observed with substantial spatial and temporal change near thunderstorms, *J. Geophys. Res. Space Physics*, **119**, 4916–4928, doi:10.1002/2013JA019430.
- Lee, J. H., and D. Kalluri (1999), Three-dimensional FDTD simulation of electromagnetic wave transformation in a dynamic inhomogeneous magnetized plasma, *IEEE Trans. Antennas Propag.*, **47**(7), 1146–1151.
- Liu, N. (2012), Multiple ion species fluid modeling of sprite halos and the role of electron detachment of O^- in their dynamics, *J. Geophys. Res.*, **117**, A03308, doi:10.1029/2011JA017062.
- Marshall, R. A. (2012), An improved model of the lightning electromagnetic field interaction with the *D*-region ionosphere, *J. Geophys. Res.*, **117**, A03316, doi:10.1029/2011JA017408.
- Marshall, R. A., U. S. Inan, and W. A. Lyons (2006), On the association of early/fast very low frequency perturbations with sprites and rare examples of VLF backscatter, *J. Geophys. Res.*, **111**, D19108, doi:10.1029/2006JD007219.
- Marshall, R. A., U. S. Inan, and T. W. Chevalier (2008), Early VLF perturbations caused by lightning EMP-driven dissociative attachment, *Geophys. Res. Lett.*, **35**, L21807, doi:10.1029/2008GL035358.
- Marshall, R. A., U. S. Inan, and V. S. Glukhov (2010), Elves and associated electron density changes due to cloud-to-ground and in-cloud lightning discharges, *J. Geophys. Res.*, **115**, A00E17, doi:10.1029/2009JA014469.
- Marshall, R. A., T. Wallace, and M. Turbe (2016), Finite difference modeling of VLF propagation in the Earth-ionosphere waveguide, Abstract SA41A-2362 presented at 2016 Fall Meeting, AGU, San Francisco, Calif., 12–16 Dec.
- Mika, A., C. Haldoupis, R. A. Marshall, T. Neubert, and U. S. Inan (2005), Subionospheric VLF signatures and their association with sprite observed during EuroSprite-2003, *J. Atmos. Sol. Terr. Phys.*, **67**, 1580–1597.
- Mika, A., C. Haldoupis, T. Neubert, R. R. Su, H. T. Hsu, R. J. Steiner, and R. A. Marshall (2006), Early VLF perturbations observed in association with elves, *Ann. Geophys.*, **24**, 2179–2189.
- Moore, R. C., C. P. Barrington-Leigh, U. S. Inan, and T. F. Bell (2003), Early/fast VLF events produced by electron density changes associated with sprite halos, *J. Geophys. Res.*, **108**(A10), 1363, doi:10.1029/2002JA009816.
- Pasko, V. P., and U. S. Inan (1994), Recovery signatures of lightning-associated VLF perturbations as a measure of the lower ionosphere, *J. Geophys. Res.*, **99**(A9), 17,523–17,537.
- Pasko, V. P., U. S. Inan, T. F. Bell, and Y. N. Taranenko (1997), Sprites produced by quasi-electrostatic heating and ionization in the lower ionosphere, *J. Geophys. Res.*, **102**(A3), 4529–4561.
- Pasko, V. P., U. S. Inan, and T. F. Bell (1998), Ionospheric effects due to electrostatic thundercloud fields, *J. Atmos. Sol. Terr. Phys.*, **60**, 863–870.
- Roden, J. A., and S. D. Gedney (2000), Convolution PML (CPML): An efficient FDTD implementation of the CFS-PML for arbitrary media, *Microwave Opt. Tech. Lett.*, **27**(5), 334–339.
- Taranenko, Y. N. (1993), Interaction with the lower ionosphere of electromagnetic pulses from lightning: Heating, attachment, ionization, and optical emissions, PhD thesis, Stanford Univ., Stanford, Calif.
- Thomson, N. R., M. A. Clilverd, and W. M. McRae (2007), Nighttime ionospheric *D* region parameters from VLF phase and amplitude, *J. Geophys. Res.*, **112**, A07304, doi:10.1029/2007JA012271.
- Wait, J. R., and K. P. Spies (1964), Characteristics of the Earth-ionosphere waveguide for VLF radio waves, Tech. Note 300, Natl. Bur. of Stand., Boulder, Colo.
- Zoghzyghy, F., M. B. Cohen, R. K. Said, and U. S. Inan (2013), Statistical patterns in the location of natural lightning, *J. Geophys. Res. Atmos.*, **118**, 787–796, doi:10.1002/jgrd.50107.